Journal of Colloid and Interface Science 336 (2009) 698–706

Contents lists available at ScienceDirect

Journal of Colloid and Interface Science

www.elsevier.com/locate/jcis

Infiltration time and imprint shape of a sessile droplet imbibing porous medium

B. Markicevic, H. Li, Y. Sikorski, A.R. Zand, M. Sanders, H.K. Navaz *

Department of Mechanical Engineering, Kettering University, 1700 West University Avenue, Flint, MI 48504, USA

ARTICLE INFO

Article history:
Received 23 January 2009
Accepted 25 April 2009
Available online 13 May 2009

Keywords:
Homogeneous porous media
Sessile droplet spread
Capillary network model
Infiltration time non-dimensional curve and imprint shape

ABSTRACT

The infiltration of a sessile droplet into a homogeneous porous medium for a constant droplet base radius case is solved numerically, where the porous medium is represented as a capillary network consisting of pores and throats. For a homogeneous medium, the network is built of the spherical pores of constant radius, and the cylindrical throats of constant radius and height. Having such defined network, the droplet imbibes porous medium in a single-phase flow for which the free interface in porous medium is smooth, and the liquid phase permeability and the capillary pressure are constant. Using the numerical solution we carry out the parametric study in which: (i) liquid viscosity and surface tension, (ii) droplet volume and base radius, and (iii) porous medium porosity and permeability are varied. The droplet infiltration time, and the imprint shape that is given with two spheroid half-axes are calculated. The dimensionless analysis is utilized to correlate the droplet infiltration parameters from which master curves for the droplet infiltration time and the droplet imprint shape are obtained. Using the infiltration time correlation, both numerical and experimental results show a linear behavior.

Published by Elsevier Inc.

1. Introduction

The infiltration of a sessile droplet of a low-volatile, non-reacting liquid into porous medium is defined as a momentum transport problem only, but still with a variety of mechanisms that need to be taken into account such as the influence of the terminal (deposition) velocity [1], the liquid spread rate at the porous medium surface [2], and the infiltration rate into the porous medium [3]. For the cases in which the terminal velocity can be neglected, the spread and infiltration rates are solely influenced by capillary force. The capillarity tends to suppress the spread of the free liquid residing on the porous medium surface, and at the same time is responsible for liquid infiltration into the porous medium [4]. Depending on the relative magnitude of the capillary forces in these two regions, the droplet spread is altered ranging from the droplet base remaining almost constant to the droplet base varying throughout the spread [5].

The liquid spread on the porous medium surface is quantified using the droplet base radius and it has been shown that it varies significantly for a complete wetting liquid, whereas it remains more constant for a partially wetting liquid [2,6] as the capillary force is reduced in the later case. Because the spread rate of the liquid on the porous medium is much higher than the infiltration rate the free droplet reaches its equilibrium dynamic constant angle [7]. On the other hand, for these two rates being comparable, the infiltration rate prevents free fluid from spreading further on the porous medium surface [5]. In order to investigate the droplet infiltration, Alleborn and Raszillier [8,9] have carried out full numerical simulations for both thin and thick porous media, where the spread is influenced by medium thickness. For thin porous medium, the liquid flow is restricted into two dimensions only. For thick media, the lubrication approximation implies that the infiltration is governed mainly by pressure gradients in the droplet protrusion direction. It is obvious that the droplet fate is influenced by both surface spread and infiltration flow [3], where the droplet can spread in a variety of scenarios including two special cases: either with the constant base radius or constant dynamic contact angle at the porous medium surface. In the model of Denesuk et al. [7], the infiltration time for both mechanisms are predicted, where the spread time is nine times longer for a constant contact angle than for a constant base radius. In this solution, the porous medium is represented as an array of parallel capillaries normal to the surface on which the sessile droplet resides and the pressure solution is obtained from Washburn's equation. Besides the infiltration time, the shape of the droplet imprint (wetted volume in porous medium) is also investigated, where the imprint shape depends on the dynamics of the droplet spread on the porous medium surface. Davis and Hocking [10,11] have solved for both shapes: free droplet and imprint geometry using the method of contact line in which they used the slip boundary condition.

The droplet infiltration is a three-dimensional flow with a radial symmetry, where the flow front advances in both directions: (i) parallel, and (ii) perpendicular to the surface on which the droplet is deposited. Having both flows taking place, the infiltration time is smaller compared to either parallel flow only (infiltration into thin

* Corresponding author. Fax: +1 810 762 7860.
E-mail address: hnavaz@kettering.edu (H.K. Navaz).

0021-9797/$ - see front matter Published by Elsevier Inc.
doi:10.1016/j.jcis.2009.04.085

Nomenclature

a_i	polynomial coefficients
A	system matrix for pressure solution, $m^3/(Pa\ s)$
b, k, m, n	dimensionless correlation coefficients, Eq. (20)
b	force vector for pressure solution, m^3/s
c	coordination number
g	throat conductance, $m^3/(Pa\ s)$
I	cosine of liquid/solid contact angle
K	permeability of isotropic medium, m^2
l_x, l_y, l_z	porous medium dimensions in x, y, and z direction, m
n_x, n_y, n_z	number of pores in x, y, and z directions
p	pressure, Pa
q	flow rate into one pore, m^3/s
Q	flow rate across macroscopic boundary, m^3/s
r	radius, m
r_0	droplet base radius, m
l	length, m
l_K	permeability length scale, $K = (1/l_K) \times (r_t^4/l_t)$, m
s	pore saturation
S	surface area, m^2
t	time, s
u	macroscopic velocity vector, m/s
V_0	initial sessile droplet volume, m^3
V_m	porous medium total volume, $l_x l_y l_z$, m^3
V_p	pore volume, m^3
V_{por}	porous medium wetted volume, m^3

Greek symbols

α, β	spheroidal imprint half-axes, m
ϕ	porosity
κ	porous medium constant in Eq. (25), $mm^{0.85}$
μ	viscosity, Pa s
σ	surface tension, Pa m
θ	liquid/solid phase contact angle in porous medium, deg
θ_d	sessile droplet dynamic contact angle at the porous medium surface, deg

Subscripts

int|Gas and int|Liq	gas and liquid phase from the interface
c	capillary
ch	characteristic
exp	experimental
i,j	pair of pores, or throat connecting pair of pores
in	infiltration
inl	inlet boundary
int	liquid interface in porous medium
mod	model
out	outlet boundary
p	pore
step	discrete step
t	throat

porous medium) or perpendicular flow only (infiltration of a medium that consists of pores that are not cross-connected). Furthermore, due to the difference in capillary forces in the clear fluid (sessile droplet) and at the imprint (porous medium wetted volume) interface, the fluid front at the porous medium surface can advance compared to the residing sessile droplet base. This causes an increase in the infiltration time due to the liquid flow through porous medium. Therefore, the infiltration time and imprint shape are numerically solved accounting for both parallel and perpendicular flows, and the presence of an advancing flow front in porous medium compared to the sessile droplet base position. Finally, from the dimensionless analysis general correlations for the infiltration time and imprint shape are obtained.

2. Problem formulation

The transport of a sessile droplet into a porous medium is comprised of an inner and an outer problem, the first being the liquid infiltration into porous medium and the latter is a free liquid spread on the porous medium surface. The solution of the overall problem is obtained by matching these two solutions across the porous medium surface [2,6]. The outer solution is known in advance for two special cases in which the droplet spread takes place under either constant base radius [3,7], or constant contact angle [7]. In these two cases, the inner problem needs to be solved only with the constraint that the volume of the infiltrated liquid is equal to the initial volume of the droplet. The inner solution for a special case of the sessile droplet constant base radius (r_0 = const.) is considered in this study. A schematic of (r_0 = const.) case is depicted in Fig. 1, where the initial droplet volume (V_0) and droplet base radius (r_0) are shown as well as the instantaneous changes of the free liquid and infiltrated volumes. At the end of the process, the infiltrated volume (V_{por}) is equal to the initial volume (V_0) divided by medium porosity (ϕ). Two contact angles between solid and liquid phases are defined: contact angle within porous medium (θ), and

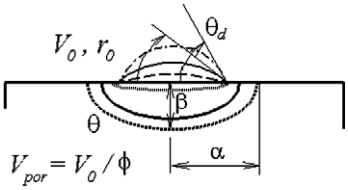

Fig. 1. Spread of the sessile droplet of initial volume (V_0) and droplet base radius (r_0) into homogeneous porous medium for (r_0 = const.). The imprint volume, $V_{por} = V_0/\phi$. Contact angle (θ) inside porous medium, dynamic contact angle (θ_d), and imprint half-axes α and β are shown.

dynamic contact angle at the porous medium surface (θ_d). Angle θ remains constant throughout the spread, whereas θ_d changes with its initial value obtained from V_0 and r_0. Finally, the droplet imprint in the porous medium is given with half-axes α and β.

During the droplet infiltration, there are parallel and perpendicular flows into the porous medium defined in the directions parallel and perpendicular to the porous medium surface on which the droplet resides. Due to the parallel flow, the radius of the liquid imprint increases in time with a lag between the imprint front and sessile droplet front on the porous medium surface. However, in a special case of a medium consisting of parallel but not cross-linked capillaries the flow occurs in perpendicular direction only. For such medium and constant droplet base radius (r_0), the analytical model for the infiltration time (t_{in}) has been developed by Denesuk et al. [7] that in non-dimensional form can be written as:

$$\frac{t_{in}\sigma}{\mu}\frac{K}{r_t^3} = \frac{1}{32\pi^2 I}\left(\frac{V_0}{r_0^2\sqrt{K}}\right)^2 \tag{1}$$

where μ and σ are liquid viscosity and surface tension, r_t is a capillary radius, and K is the porous medium permeability. The constant I is calculated from the surface tension action at the tri-point of the gas (G), liquid (L), and solid (S) phases, and it is equal to

$I = (\sigma_{SG} - \sigma_{SL})/\sigma_{LG}$, that defines the cosine of the equilibrium contact angle. The model can be also used for constant contact angle, where the infiltration time is nine times longer compared to (r_0 = const.) case. It can be seen from Eq. (1) that the porosity (ϕ) does not influence (t_{in}) as it is included in the areal density of the capillaries (integrated in the model development). For porous media with both parallel and perpendicular flow in which the capillaries are cross-linked to some extent, Navaz et al. [12] have shown that the porosity influences the infiltration time, where the solution is given as a family of infiltration time curves as a function of the dynamic contact angle with porosity as a parameter.

There are two groups of parameters: kinetic (μ, σ, K, r_t) and dynamic (V_0, r_0, ϕ) that influence the droplet infiltration process. Both of them influence the infiltration time, whereas dynamic parameters influence the shape of the droplet imprint in the porous medium. Similarly to the previous studies, the infiltration time depends on:

$$t_{in} = \psi(\mu, p_c, V_0, r_0, K, \phi, r_t, l_{ch}) \tag{2}$$

where p_c is the capillary pressure, l_{ch} is characteristic length of droplet/porous medium interactions, and all other parameters are as given previously. It should be noted here that besides permeability (K), two additional parameters of the porous medium (ϕ, r_t) are included as the porosity is a storage property of the porous medium, and the permeability is at least the function of two parameters. From dimensional analysis, Eq. (2) can be recast in the next dimensionless form:

$$\frac{t_{in} p_c}{\mu} \frac{K}{l_{ch}^2} \phi^m = b \left(\frac{V_0}{r_0^3} \right)^k \tag{3}$$

with b, k, and m model constants to be calculated from the numerical or experimental data. Furthermore, adopting the spheroid geometry [13], the imprint shape is given with two half-axes lengths α and β that are functions of (V_0, r_0, ϕ) only. The imprint volume is equal to $V_{por} = V_0/\phi$ and from the mass balance one can write:

$$\frac{V_0}{\phi} = \frac{2\pi}{3} \alpha^2 \beta \tag{4}$$

In order to solve for α and β from Eq. (4), the dependence $\alpha = f(\beta, r_0)$ needs to be determined.

3. Numerical solution

In the current study, the porous medium is considered to be homogeneous and isotropic, and therefore, the droplet infiltration is solved as a single-phase flow with a free moving boundary. In this flow, the liquid interface in the porous medium is smooth with sharply separated, fully saturated and non-saturated regions within the porous medium. Therefore, the liquid phase permeability is constant and equal to the medium permeability (K). Across the interface (gas|liquid), there is a pressure jump due to the capillary pressure (p_c) that, again, due to non-varying saturation (equal to one at the interface) is constant. The droplet infiltration is a free boundary flow, where the instantaneous wetted volume (V_{por}) change in the porous medium is calculated from the liquid velocity at the free interface ($\mathbf{u}_{int}$). Combining the continuity and the Darcy law with the pressure jump condition and free-surface flow the next set of equations describes the sessile droplet infiltration into porous medium [14]:

$$\nabla \cdot \mathbf{u} = 0 \tag{5}$$

$$\mathbf{u} = -\frac{K}{\mu} \nabla p \tag{6}$$

$$p_c = p_{int|Gas} - p_{int|Liq} \tag{7}$$

$$dV_{por}/dt = \int_{S_{int}} \mathbf{u}_{int} \cdot dS \tag{8}$$

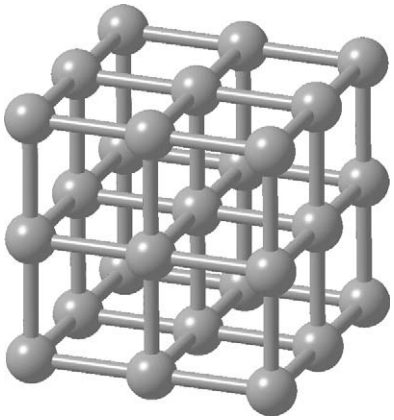

Fig. 2. A schematic of the homogeneous regular cubic capillary network in which all pores (spheres) and throats (cylindrical connections) are, each, of the same sizes.

where $\mathbf{u}$ and p are velocity and pressure in liquid phase, and index ($_{int}$) refers to the quantity at the interface.

Eqs. (5)–(8), are solved on the domain that is represented as a homogeneous capillary network that consists of pores and throats each being of equal size. Such network is shown in Fig. 2, where each pore is connected to its six neighboring pores giving the network coordination number equal to six. Writing the mass balance from Eq. (5) over one pore (i) as a sum of flow rates (q_j), and the momentum balance from Eq. (6) for the throat (i, j) of conductance (g) which connects pores (i) and (j), and pore pressures (p_i) and (p_j):

$$\sum_{1 \leqslant j \leqslant c} q_{i,j} = 0 \tag{9}$$

$$q_{i,j} = \frac{\pi r_t^4}{8 \mu l_t} (p_j - p_i) = g \Delta p_{i,j} \tag{10}$$

After assembling for all pores that are wetted by liquid, the linear system of algebraic equations is obtained. The coefficient matrix $\mathbf{A}$ depends on the throat conductance (g), and the force vector ($\mathbf{b}$) is a function of g, external pressures (p_{inl}) and (p_{out}), and the capillary pressure ($2\sigma\cos(\theta)/r_t$). Hence, the pressure of the liquid phase ($\mathbf{p}$) is found solving:

$$\mathbf{A}(g) \cdot \mathbf{p} = \mathbf{b}(g, p_{inl}, p_{out}, 2\sigma \cos(\theta)/r_t) \tag{11}$$

Two types of pores can be identified at the boundary: (i) pores next to the sessile droplet base – inlet boundary (S_{inl}), and (ii) pores at the free interface (S_{int}) within porous medium. The capillary pressure jump condition in Eq. (7) applies to the pores at (S_{int}). For the boundary pore (i), the flow rate (q_i) for one pore reads as:

$$q_i = \begin{cases} g(p_{inl} - p_i), & \text{at } S_{inl} \\ \sum\limits_{1 \leqslant j \leqslant c_{int}} g(p_{out} - 2\sigma \cos(\theta)/r_t - p_j), & \text{at } S_{int} \end{cases} \tag{12}$$

The pore that belongs to S_{inl} is connected to sessile liquid by one throat. Each pore at S_{int} is connected to c_{int} pores, where c_{int} is the interface pore coordination number of throats occupied by the liquid phase. It should be noted here that for pores at S_{int}, the coordination number c_{int} varies, and is different from the network coordination number c. The pores at the porous medium boundary between droplet base and wetted imprint front (leg length in Fig. 1) belong to (S_{int}) if partially saturated. Otherwise, they belong to the liquid body if fully saturated. Finally, the mass conservation is insured provided that the flow rates (Q) across the inlet boundary (S_{inl}) and interface (S_{int}) are equal:

$$Q = \sum_{S_{inl}} q_{inl,i} = \sum_{S_{int}} q_{int,i} \tag{13}$$

The time needed to fill any of the pores at the interface (S_{int}) can be calculated from the pore volume (V_p), the pore volume fraction that is filled by displacing liquid (pore saturation), and the flow rate into the pore:

$$t_i = (1 - s_i)V_p/q_i \tag{14}$$

In order to track the interface dynamics the calculated fill times for all pores at the interface (t_i), ($1 \leqslant i \leqslant n_{int}$) are compared, and the minimum time for which pore(s) at the interface become(s) full is defined as the discrete time step (t_{step}),

$$t_{step} = \min_{1 \leqslant i \leqslant n_{int}} \{t_i\} \tag{15}$$

This time step is used to calculate the volume of the liquid that flows into the porous medium (V_{step}) in a current step multiplying the liquid flow rate (Q) across the inlet (q_{inl}) (or q_{int}, see Eq. (13)) by t_{step} (Eq. (8)). In the next step, a new interface is identified and the calculations shown in Eqs. (12)–(15) are repeated. In each time step, the flow rate across the inlet (or interface) changes in time $Q(t)$, and the infiltration is terminated once the integrated $Q(t)$ in time is equal to the droplet initial volume (V_0). The sum of all t_{step} gives the infiltration time (t_{in}) of sessile volume (V_0). Finally, the spheroid wetted imprint half-axes α and β for V_0 (and so t_{in}) are computed from the known interface position after (V_0) has infiltrated the porous medium.

An actual porous medium and its parameters: porosity (ϕ), permeability (K), and capillary pressure (p_c) are related to a network by distinguishing the porous medium storage and transport properties. Thus, for the network of size ($n_x \times n_y \times n_z$), the pore volume ($V_p$) is calculated from the overall medium volume (V_m) and porosity (ϕ):

$$V_p = V_m\phi/(n_x \times n_y \times n_z) \tag{16}$$

The transport properties K and p_c are found from the network remaining two parameters, throat radius (r_t) and throat length (l_t). From the Poiseuille solution and Young–Laplace equation K and p_c scale as:

$$K \propto r_t^4/l_t \quad \text{and} \quad p_c \propto 1/r_t \tag{17}$$

where in p_c the contact angle (θ) between the liquid and solid phase of porous medium is set equal to zero. Since the porous medium is homogeneous, θ greater than zero would reduce the capillary pressure and increase infiltration time and dividing by $\cos(\theta)$ would produce the infiltration time calculated for ($\theta = 0$). This is true as long as θ does not depend on the liquid flow rate. From Eqs. (16) and (17), the problem is well posed as the medium parameters (ϕ, K, p_c) are replaced by network parameters (V_p, r_t, l_t). With respect to the sessile droplet, the base radius (r_0) is correlated to the network parameters, where for a porous domain ($l_x \times l_y \times l_z$) and network size ($n_x \times n_y \times n_z$) the equivalent length (l_{eq}) is defined such that $l_{eq} = l_i/n_i$, $i = \{x, y, z\}$. Therefore, the droplet base radius expressed in number of pores is equal to (r_0/l_{eq}).

4. Results and discussion

The infiltration time (t_{in}) and imprint shape given with two half-axes α and β of the sessile droplet into porous medium are calculated using the homogeneous network. In the numerical calculations, all there groups of parameters are varied: (i) liquid properties – viscosity (μ) and surface tension (σ), (ii) sessile droplet parameters – droplet volume (V_0) and base radius (r_0), and (iii) porous medium properties – porosity (ϕ) and permeability (K). In the numerical calculations, r_0 was set equal to $r_0 = \{1, 2, 3, 4\}$ mm and the initial volume (V_0) was varied from equal to zero to $V_0 = 2\pi r_0^3/3$ which gives the dynamic contact angle on the porous medium surface from zero to $\pi/2$ (note that the dynamic contact angle differs from the contact angle in the porous medium that was set equal to zero in this study). Three different values for the porosity were used, $\phi = \{0.2, 0.5, 0.8\}$ and the permeability of the network is varied in five orders of magnitude range that were obtained by setting network parameters (r_t) and (l_t). Finally, in each case that was investigated the droplet base radius (r_0) remains constant throughout the infiltration (Fig. 1).

The values of r_t and l_t are set equal to $r_t = \{0.64, 1.6, 4, 10, 25\}$ μm and $l_t/r_t = \{0.256, 0.48, 1, 1.6, 3\}$ and in order to calculate network permeability, the fully saturated flow through the network is solved. The permeability is calculated from the Darcy law that correlates the flow rate (q) and the pressure drop (Δp) given with:

$$\frac{q}{n_x n_y l_{eq}} = \frac{K}{\mu}\frac{\Delta p}{n_z} \tag{18}$$

where the flow is unidirectional in z direction and l_{eq} is the network length equivalent explained earlier. It can be seen from Eq. (17) that permeability (K) scales with (r_t^4/l_t) and additional length scales (l_K) need to be introduced into permeability expression. The physical meaning of the constant (l_K) is that more than one porous medium can have the same (r_t, l_t), but still different permeabilities (K). The variation in permeability is caused by medium structure where the site pore coordination number (c) is defined as a number of neighboring pores connected to the site pore. The value of (c) can be constant (each site pore connected to the same number of neighbors), or vary throughout the medium that can be defined by using (c) distribution function. For a network in Fig. 2 with a constant coordination number (in this study equal to six), (l_K) should remain constant and $K = (1/l_K) \times (r_t^4/l_t)$. The permeability ($K$) results for all 25 pairs of (r_t, l_t) and how K changes as a function of (r_t^4/l_t) are given in Fig. 3 in which the linear dependence is observed (*log*-axes are used just for better representation). From the least square regression, it is found that $l_K = 2.58 \times 10^{-4}$ m for a regular cubic network as the one depicted in Fig. 2.

The numerical results for t_{in} are correlated as given in Eq. (3). Initially, the influence of liquid properties μ and σ on t_{in} is investigated. For a specific porous medium with a known throat radius of r_t, the capillary pressure is equal to $p_c = 2\sigma/r_t$ for a completely wetting liquid (contact angle within porous medium, $\theta = 0$ and $\cos(\theta) = 1$). For two liquids with different contact angles (θ), (p_c) is reduced by $\cos(\theta)$, i.e., $p_c = 2\sigma\cos(\theta)/r_t$. As long as θ does not de-

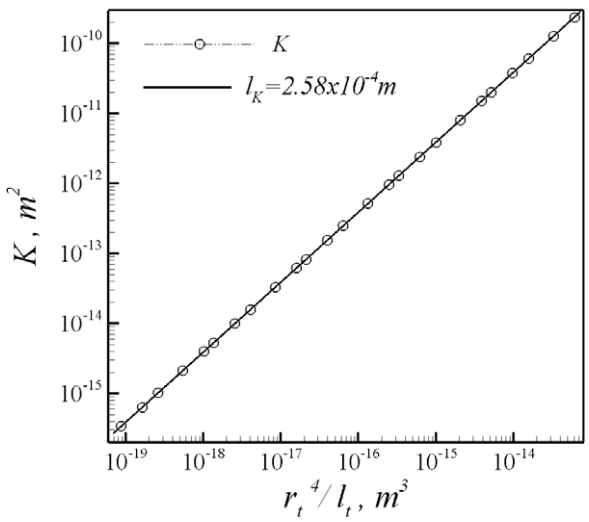

Fig. 3. Permeability of the homogeneous regular cubic capillary network (coordination number equal to 6) as a function of the network parameters (r_t^4/l_t) with the network constant (l_K), $K = (1/l_K) \times (r_t^4/l_t)$.

pend on the infiltration rate, $\sigma\cos(\theta)$ is a constant for a pair of porous medium and liquid, thus the term $(t_{in}p_c/\mu)$ can be replaced by $(t_{in}\sigma/\mu)$. The starting of μ and σ are water values, and thereafter: (i) viscosity, (ii) surface tension, and (iii) both μ and σ are increased for an order of magnitude. As suggested from Eq. (3) and models of Denesuk et al. [7] and Navaz et al. [12] the group $(t_{in}\sigma/\mu)$ collapses the infiltration time on the same value irrespective of μ and σ. The numerical results for $(t_{in}\sigma/\mu)$ as a function of (V_0/r_0^3) and four distinct pairs (μ, σ) investigated are shown in Fig. 4 for $\phi = 0.5$ and $r_0 = 2$ mm. Besides t_{in}, the imprint half-axes α and β are also calculated, and as expected they are not influenced by μ and σ as shown in Fig. 5. Here, μ and σ influence the infiltration time, but not the volume to be filled (α and β). For small (V_0/r_0^3) droplets, there is a large aspect ratio of α to β as the liquid is smeared on the porous medium surface and protrusion depth (β) is small. For larger initial dynamic contact angle on the porous medium surface and so larger V_0/r_0^3, α to β ratio becomes comparable and droplet imprint becomes close to spherical in shape.

In Fig. 4, the network permeability (K) is defined setting $r_t = 0.64$ μm, $l_t/r_t = 0.256$. The infiltration time is influenced by K, where Eq. (3) suggests that t_{in} and K are linearly dependent in the form $(t_{in}p_cK/\mu)$. The group $(t_{in}\sigma/\mu)$ unifies all t_{in} results with respect to μ and σ, and from Eq. (17) for K and p_c scales, it can be written:

$$\frac{t_{in}}{\mu}p_cK \approx \left|\begin{matrix} K \propto r_t^4/l_t \\ p_c \propto 1/r_t \end{matrix}\right| \approx \frac{t_{in}\sigma}{\mu}\frac{r_t^3}{l_t} \tag{19}$$

Having defined $p_c \times K$ scale to be proportional to (r_t^3/l_t), the infiltration time (t_{in}) of a droplet of $r_0 = 3$ mm into a medium of porosity $\phi = 0.5$ is calculated for 25 different combinations of (r_t, l_t), the same one as in the network permeability prediction (see Fig. 3). The values of r_t and l_t are chosen to give a large variation in the permeability ($K = 10^{-15}$–10^{-10} m^2) and the infiltration time (t_{in}) thereafter, because K and t_{in} are linearly proportional. Furthermore, r_t and l_t are set to produce 17 distinct values of (r_t^3/l_t), and conversely (r_t^4/l_t) produces 25 different values as can be seen from Fig. 3. Hence, varying the droplet initial volume (V_0) from zero to $2\pi r_0^3/3$ and plotting the infiltration time (t_{in}) as a function of (V_0/r_0^3) gives 17 different curves as shown in Fig. 6a. Since (t_{in}) changes for a few orders of magnitude (due to the changes in network permeability) the results are given in a *log–log* plot. In Fig. 6b, the data are reduced into the form as given in the right hand side of Eq. (19), where the single curve is obtained. From the form of curve in Fig. 6b, it can be seen that the infiltration rate is greater for the droplet that is more spread on the porous medium surface (small V_0/r_0^3). However, in *log–log* plot this dependence is a straight line (Fig. 6a) suggesting that t_{in} is a power function of V_0/r_0^3 as proposed in Eq. (3) with the exponent k. From the regression, it is found that $(k = 1.45)$ and this linear dependence is shown in Fig. 6c, in which the numerical data are given with symbols and the power function $(V_0/r_0^3)^k$ is represented with thick solid line.

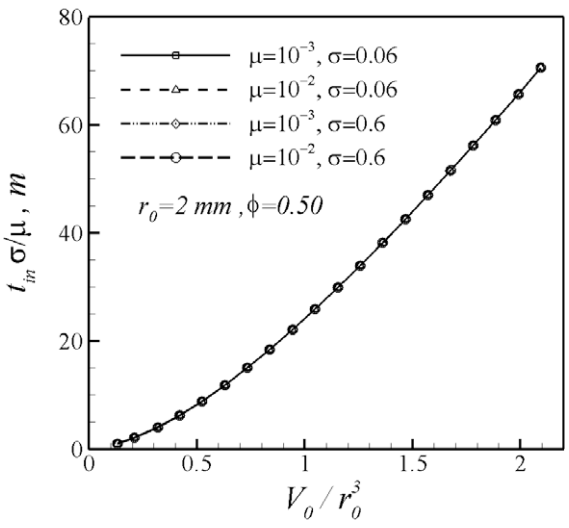

Fig. 4. Reduction of the sessile droplet infiltration time for four different combinations of fluid viscosity (μ, in Pa s) and surface tension (σ, in Pa m).

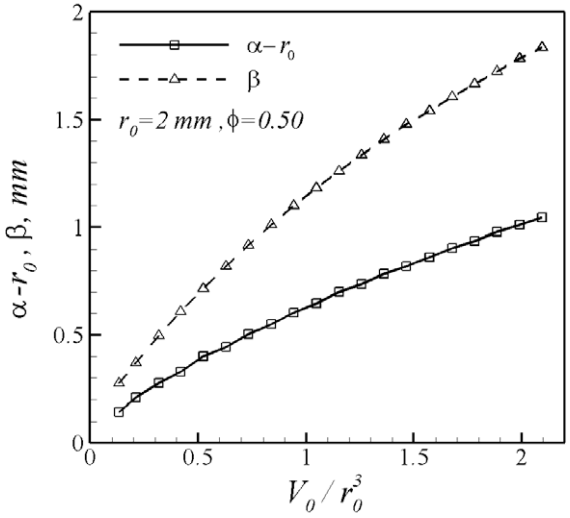

Fig. 5. Imprint geometry change given with the spheroid half-axes α and β as a function of the droplet initial volume (V_0) for four distinct (μ, σ) (same values as in Fig. 4). Note that α and β are not influenced by liquid properties (μ) and (σ).

4.1. Dynamic parameters (ϕ, r_0)

The porosity (ϕ) defines a storage property of porous medium and in the network is expressed through the pore volume (V_p) calculated from Eq. (16). As ϕ decreases, both imprint shape (V_{por}) and infiltration time (t_{in}) increase. In order to check the assumption that t_{in} is a porosity power function (ϕ^m), the set of the numerical results for $r_0 = 2$ mm and porosity $\phi = \{0.1, 0.2, \ldots, 0.9\}$ is carried out, where t_{in} should be a linear function of $(V_0/r_0^3)^k, k = 1.45$. Fig. 7a shows reduced results in a form of the family of lines which after multiplying by ϕ^m, $m = 0.38$ produces a single curve for $(t_{in} \times \phi^m)$ as can be observed in Fig. 7b. Furthermore, in order to obtain a master curve of t_{in} the influence of droplet base radius (r_0) has to be accounted for which is given as a characteristic length (l_{ch}) in Eq. (3). For this purpose, in the numerical simulations r_0 and V_0 are varied and other parameters are kept constant ($\phi = 0.8$, $r_t = 0.64$ μm, $l_t/r_t = 0.256$) calculating (t_{in}). Fig. 8a summarizes the numerical results, where the family of t_{in} as a function of V_0/r_0^3 is given with r_0 as a parameter. There are only two length scales $\{r_0, l_K\}$ that can be used for l_{ch} as throat scales $\{r_t, l_t\}$ are already used for permeability reduction. Also from Eq. (3), replacing $p_c \times K$ by $\sigma \times r_t^3/l_t$ the characteristic length scales with l_{ch}^3. Using $(l_{ch} = r_0)$, the results from Fig. 8a cannot be reduced onto the single master curve, and therefore, the characteristic length (l_{ch}) is set as a combination of r_0 and the permeability length scale l_K such that $l_{ch}^3 = r_0^n \times l_K^{3-n}$, where for n equal to $n = 1.85$ all numerical results follow a single curve that is given in a linear form in Fig. 8b.

4.2. Infiltration time and imprint shape

Based on the previous consideration of how the physical parameters (liquid, droplet, and porous medium) influence the infiltration time, Eq. (3) can be written in a form that collapses all

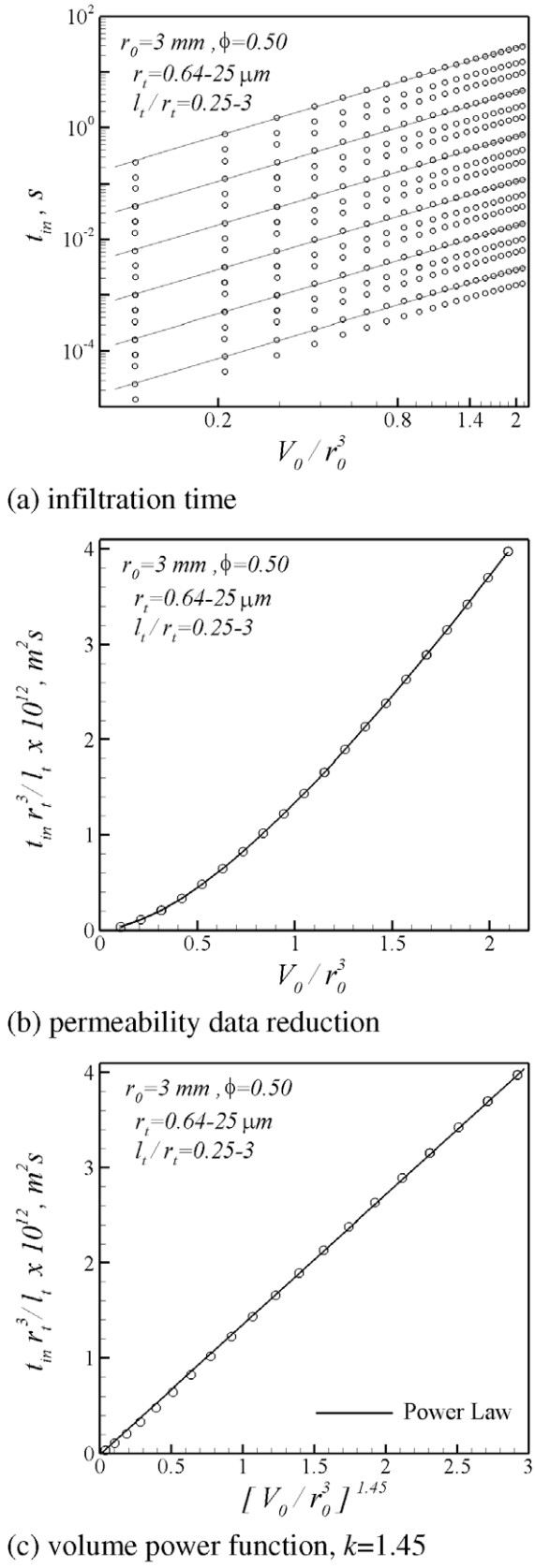

Fig. 6. Changes of the infiltration time: (a) network permeability dependence, (b) data reduction using network parameters (r_t^3/l_t), and (c) volume (V_0) to droplet base radius (r_0) power function linearization $(V_0/r_0^3)^k, k = 1.45$.

spread scenarios onto a single master curve irrespective of (μ, σ, V_0, r_0, r_t, l_t, ϕ) as follows:

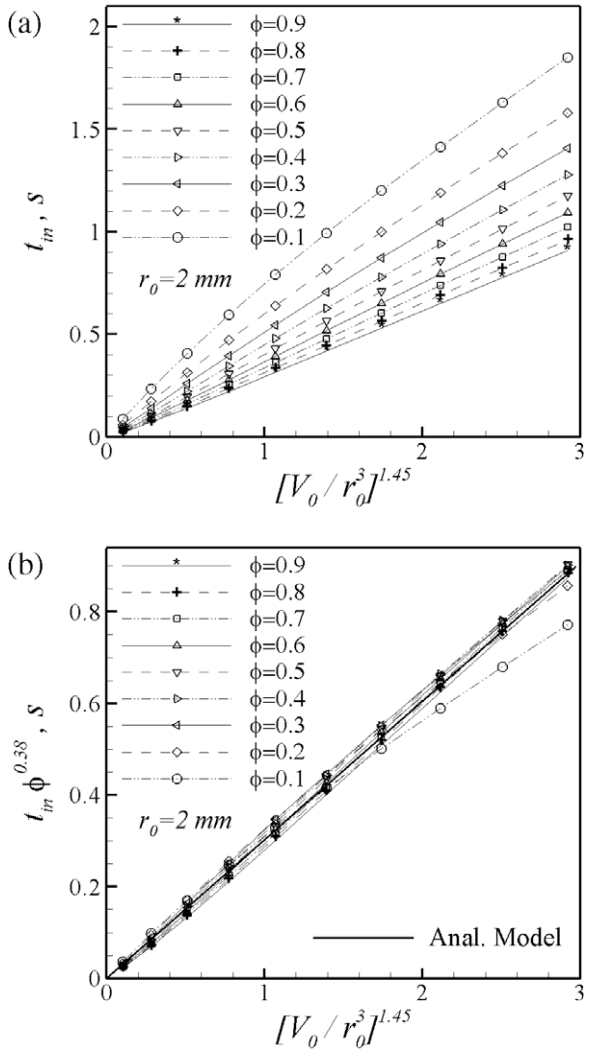

Fig. 7. Determination of the porosity power function (ϕ^m) for infiltration time: (a) linearized $(V_0/r_0^3)^k$ form for nine different porosities, and (b) single linear dependence using ($m = 0.38$).

$$\frac{t_{\text{in}}\sigma}{\mu}\frac{1}{r_0^n l_K^{3-n}}\frac{r_t^3}{l_t}\phi^m = b\left(\frac{V_0}{r_0^3}\right)^k \tag{20}$$

where $k = 1.45$, $m = 0.38$, and $n = 1.85$. Here, the properties $K(r_t, l_t)$ and $p_c(\sigma, r_t)$, and therefore, the product $(p_c \times K)$ can be expressed from (r_t, l_t, σ). More than 5000 different scenarios are carried out and Fig. 9 shows the overall comparison. The infiltration time (t_{in}) for different r_0 and ϕ as a function of V_0/r_0^3 is given in Fig. 9a. Three distinct porosities are shown using different symbols, whereas the infiltration curves for different r_0 are pointed out by using arrows. The numerical results (symbols) are connected with thin lines just for better visibility of each t_{in} curve. The data reduction proposed in Eq. (20) with exponents (k, m, n) calculated previously is given in Fig. 9b, where again the symbols represent numerical results and thick dashed and dashed double dotted lines show lower and upper limits of reduced numerical data. Only the values of coefficient (b_{lo} and b_{up}) vary in this comparison and the exponents (k, m, n) remain the same. Using $b = 0.0385$, the final expression for t_{in} is obtained and is depicted in Fig. 9b with a solid line. Two important features of t_{in} can be observed from the numerical results. The first one can be seen from Fig. 9b that for larger droplets such as $r_0 = 3$ mm, and $\phi = 0.2$ or $r_0 = 4$ mm and $\phi = 0.8$, t_{in} departs from Eq. (20) as the droplet

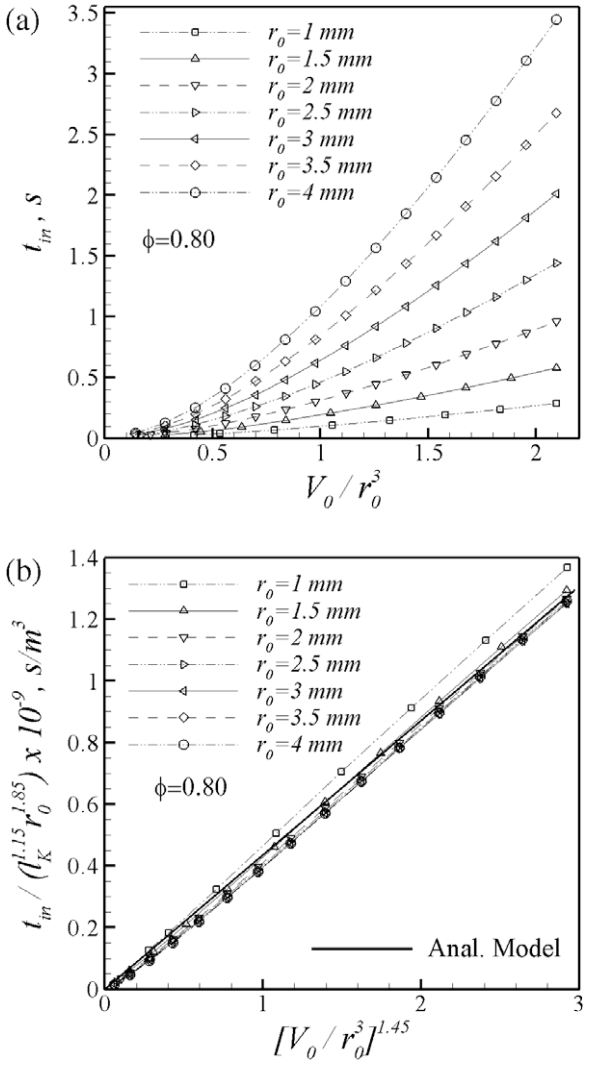

Fig. 8. Infiltration time (t_{in}) data reduction for distinct droplet base radius (r_0): (a) dependences (V_0/r_0^3), and (b) power function ($1/r_0^n$), $n = 1.85$. In order to obtain (t_{in}) dimensionless, a scale ($1/l_K^{3-n}$) is used.

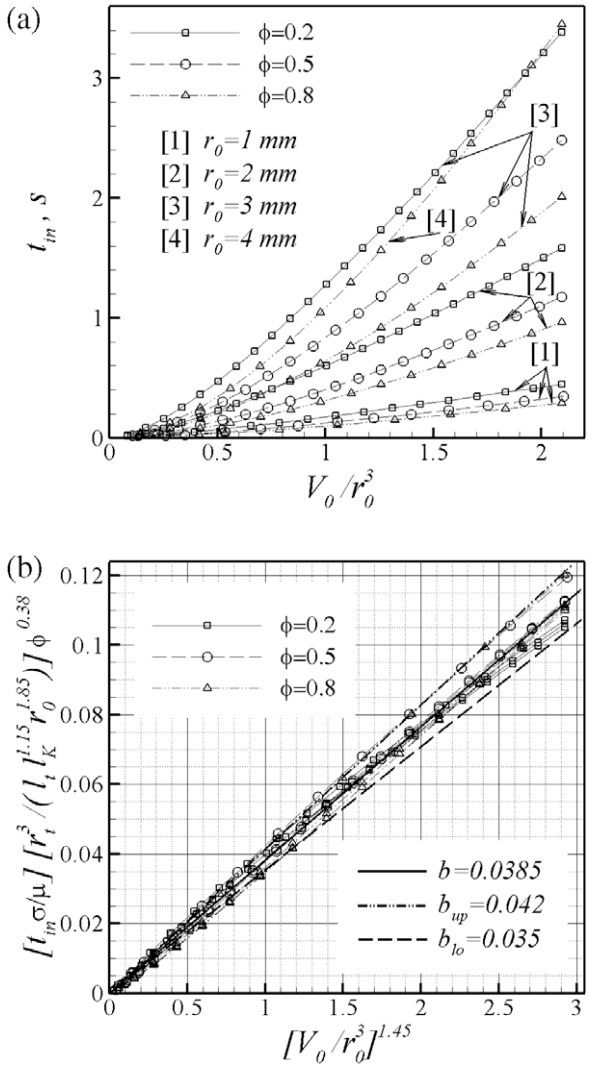

Fig. 9. Numerically calculated infiltration times shown with symbols and connected with thin lines for different $\phi = \{0.2, 0.5, 0.8\}$ and $r_0 = \{1, 2, 3, 4\}$ mm (a), and their comparison with dimensionless correlation from Eq. (20) given with thick solid line (b). The lower and upper bounds of Eq. (20) are also shown.

becomes more spherical and approaches a problem of a point spread into porous domain. The second feature that can be concluded from the form of Eq. (20) suggests that besides other parameters, t_{in} is influenced by porous medium pore connectedness that is quantified by l_K that is determined for the regular cubic networks. In this case the network coordination number is equal to six. Recasting the left hand side of Eq. (20) into the form given in Eq. (3), one obtains:

$$\frac{t_{in}\sigma}{\mu}\frac{1}{r_0^n l_K^{3-n}}\frac{r_t^3}{l_t} = \frac{t_{in}p_c}{\mu}\frac{1}{r_0^n l_K^{2-n}}K \tag{21}$$

which reveals that droplet infiltration time is indeed influenced by product ($p_c \times K$) [6], but porous medium parameter (l_K) cannot be excluded from the expression for t_{in}.

The results for the imprint shape given with two half-axes (α) and (β) are also correlated. Fig. 10 comprises the numerical results (symbols) and linear correlation (solid line) between α and β in the form:

$$\beta = \sqrt{3}(\alpha - r_0) \tag{22}$$

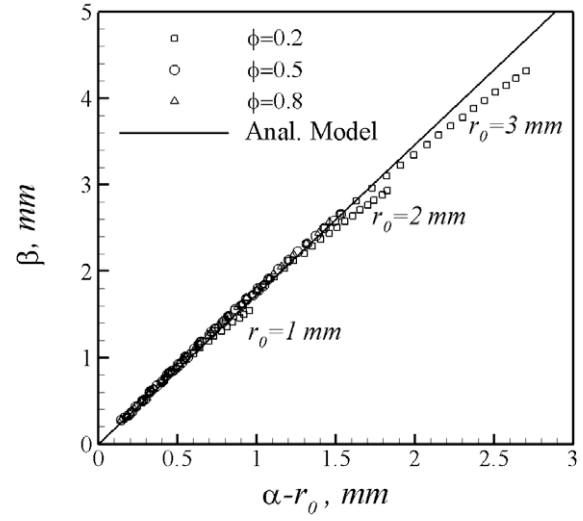

Fig. 10. Linear relationship between imprint half-axes α and β obtained from numerical solution (symbols) and prediction from Eq. (23) (solid line).

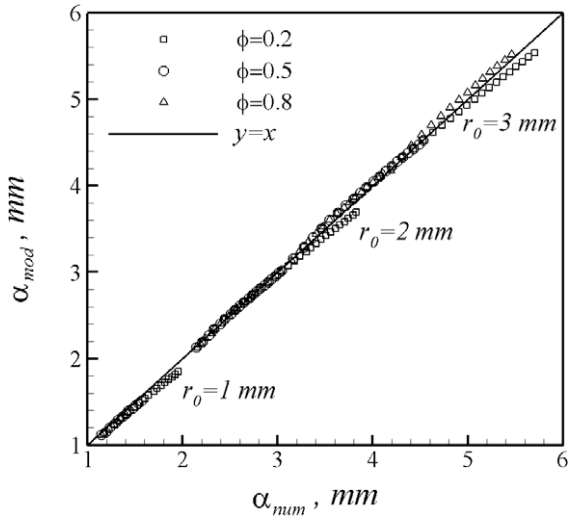

Fig. 11. Correlation between major half-axis found from numerical results (α_{num}) and (α_{mod}) predicted from Eq. (24). Solid line represents $y = x$ symmetry line.

where β is the half-axis in protrusion depth. Replacing β from Eq. (22) into Eq. (4) a cubic equation for α, $a_0\alpha^3 + a_1\alpha^2 + a_2\alpha + a_3 = 0$ and $a_0 = 1$, $a_1 = -r_0$, $a_2 = 0$, $a_3 = -V_0 3^{1/2}/(2\pi\phi)$, is obtained:

$$\alpha^2(\alpha - r_0) = \frac{V_0\sqrt{3}}{2\pi\phi} \tag{23}$$

with value of α determined using cubic formula (note that the polynomial coefficient for $a_2\alpha$ is equal to zero, $a_2 = 0$):

$$\alpha = \frac{r_0}{3} + \left[\frac{r_0^3}{27} + \frac{c}{2} + \sqrt{c\left(\frac{r_0^3}{27} + \frac{c}{4}\right)}\right]^{1/3} + \left[\frac{r_0^3}{27} + \frac{c}{2} - \sqrt{c\left(\frac{r_0^3}{27} + \frac{c}{4}\right)}\right]^{1/3} \tag{24}$$

and $c = -a_3 = V_0 3^{1/2}/(2\pi\phi)$ is equal to the right hand side of Eq. (23). The predictions of Eq. (24) for α_{mod} are compared with the numerical results (α_{num}) as shown in Fig. 11. In overall, there is an excellent correlation between α_{num} and α_{mod} as all points are close to the symmetry line $y = x$. As in Fig. 10, the distinct porosities are shown using different symbols (square, circle, and triangle for $\phi = 0.2$, 0.5, and 0.8, respectively). Even for a low porosity $\phi = 0.2$ and high V_0/r_0 there is no large deviation from $y = x$ line as cubic root expression in Eq. (24) suppress the error of Eq. (23) as the aspect ratio (α/β) becomes closer to one and the more spherical imprint shape is observed.

Finally, the master curve in Eq. (20) is compared against the experimental results of Hapgood et al. [3]. Table 1 contains the values of liquid viscosity (μ), surface tension (σ), and advancing contact angle within porous medium, (θ). In Table 1, values marked by (#) are assumed as they are not reported in [3]. It can be observed from Table 1 that there is a large change in the liquid viscosity (for

Table 1
Liquid viscosity (μ), surface tension (σ), and liquids contact angles inside porous media (θ) as reported in Hapgood et al. [3]. Values marked (#) are not listed in [3] and they are assumed.

	μ (mPa s)	σ (mPa m)	θ (deg)	
			AI glass	UQ lact.
Water	1.1	72.1	52	63#
Sat. sol.	1.1	71.6	–	63
NDBS	1.1	31	52	64
PEG200	63.8	43.7	65	64
PEG600	152.9	43.7	68	64#

Table 2
Porous medium porosity (ϕ), droplet volume (V_0), experimental time ($t_{p,exp}$), and predicted infiltration time ($t_{p,Hap}$) from [3]. Droplet base radius (r_0) calculated for initial dynamic contact angle ($\theta_d = \pi/2$) and infiltration time calculated from Eq. (25) are also tabulated.

Porous med.	Liquid	ϕ	V_0 (mm^3)	r_0 (mm)	$t_{p,exp}$ (s)	$t_{p,Hap}$ (s)	$t_{p,Eq25}$ (s)
AI glass	Water	0.45	11.6	1.76	0.63	0.15	0.09
		0.42	8.5	1.59	0.45	0.13	0.07
	NDBS	0.52	8.3	1.58	0.65	0.21	0.16
	PEG200	0.49	5.7	1.39	6.9	11.7	7.6
		0.43	5.5	1.38	5.8	13.3	7.8
	PEG600	0.47	5.6	1.38	17.4	32.5	20.6
		0.4	5.7	1.39	18.6	39.8	22.1
UQ lact.	Water	0.61	9	1.62	0.67	0.22	0.11
		0.5	10	1.68	0.56	0.15	0.13
	Sat. sol.	0.55	8.1	1.56	0.61	0.36	0.11
	NDBS	0.63	6.9	1.48	0.72	0.2	0.22
	PEG200	0.61	5.7	1.39	9.6	16	8.3
		0.48	6.3	1.44	10.7	10.4	9.6
	PEG600	0.59	5.7	1.39	21.7	35.3	20.1
		0.49	6	1.42	27.5	24.8	22.3

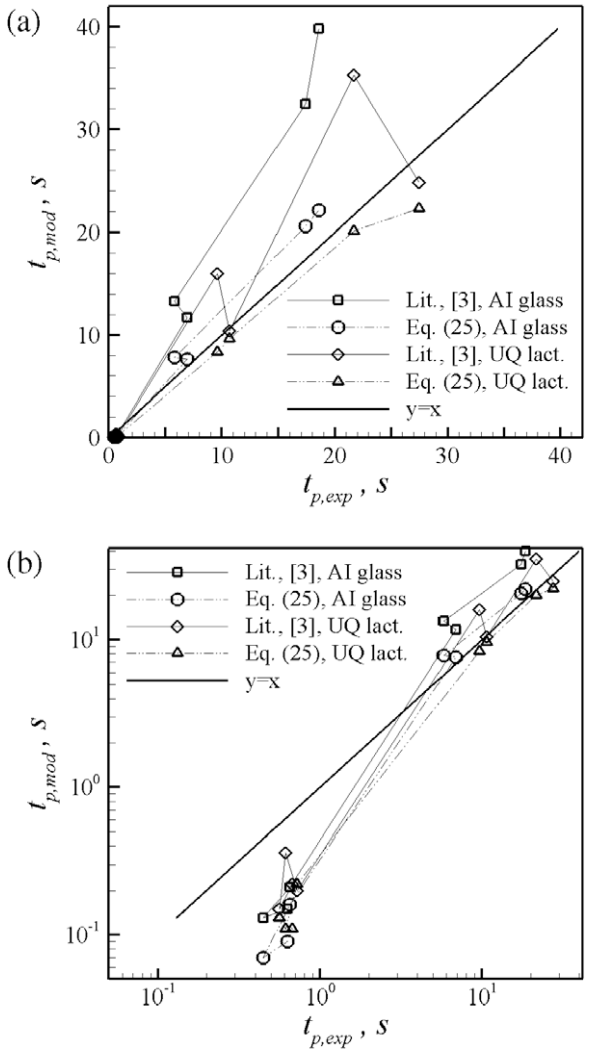

Fig. 12. Experimental and predicted infiltration times of Hapgood et al. [3] and infiltration times predicted from Eq. (25): (a) linear axes, and (b) *log*-scale axes.

almost two orders of magnitude). The angle θ remains constant throughout the infiltration and is different than the dynamic contact angle at the porous medium surface (θ_d) (see Fig. 1). In order to use Eq. (20) to predict the infiltration time, the medium permeability (K) and droplet base radius (r_0) that is found from initial (θ_d) are required and they are not reported in [3]. Taking initial $\theta_d = \pi/2$, Eq. (20) can be rewritten into:

$$t_{in} = \kappa \frac{\mu \cdot r_0^{1.85}}{\sigma \cos(\theta) \cdot \phi^{0.38}} \tag{25}$$

where $\kappa(V_0, r_0, K, l_K)$ is a constant for a specific porous medium (K, l_K) and $V_0/r_0^3 = 2\pi/3$. Table 2 summarizes the results of Hapgood et al. [3] for medium porosity (ϕ), initial droplet volume (V_0), and experimental and model predicted infiltration time (t_p is used in [3]). After calculating r_0, the infiltration time is also calculated from Eq. (25) with κ equal to 0.91 and 1.12 $mm^{0.85}$ for AI glass and UQ lactose, and listed in Table 2. The comparison between experimental ($t_{p,exp}$) and predicted infiltration times ($t_{p,mod}$) is also shown in Fig. 12 for both linear and *log*-scale axes, where different symbols represent cases investigated. As can be seen from Fig. 12, ($t_{p,mod}$) deviates from ($t_{p,exp}$) as results are off the symmetry line, $y = x$ (thick solid line) with results for PEG200 and PEG600 are closely predicted from Eq. (25). Given the findings in Fig. 9b where the results for different (r_0) are reduced onto the same master curve, the comparison in Fig. 12 suggests that other liquids used in [3] show different initial (θ_d), and therefore (r_0), that shifts the infiltration time results closer to the experimental values. This would be true if higher liquid viscosity (μ) enhances the droplet spread on the porous medium surface, and r_0 increases with μ. From Eq. (25) and Fig. 12, the value of κ needs to be recalculated based on the data for small values of μ (currently, in Fig. 12, κ is found from high values of μ). Thus, for high values of μ, the droplet base radius (r_0) increases and as given in Eq. (25), the infiltration time (t_{in}) increases as well. The changes in infiltration dynamics for small and large values of μ is corroborated from Table2. For NDBS/UQ lactose and PEG200/UQ lactose (V_0 is equal to 6.9 and 6.3 mm^3, respectively), the infiltration time increases by approximately fifteen times, although the viscosity changes by a factor of 60.

5. Conclusions

The infiltration of the wetting sessile droplet into porous medium is solved numerically using a homogeneous capillary network in which the infiltration time and the imprint shape are determined. Both liquid flows within porous medium: (i) parallel to the surface where the droplet is deposited, and (ii) perpendicular, in the direction of protrusion depth are accounted for. Due to the parallel flow, the imprint radius increases throughout the spread. For the droplet constant base radius, the droplet infiltration time is at least a seven-parameter function. These parameters are reduced using the dimensionless analysis, where the infiltration time is a function of liquid and porous medium properties, and droplet geometry. The exponents in the non-dimensional correlation are found from the numerical results, where more than 5000 different infiltration cases are reduced on a single master curve. Furthermore, the imprint (wetted porous medium) shape is found by calculating the imprint shape radius and protrusion depth. A linear relationship between these two half-axes is found and from the imprint spheroid geometry, the imprint shape radius is determined from the droplet initial volume. A very good agreement between this analytic solution and numerical results is observed. Finally, Eq. (25) is checked against experimental results where reduced infiltration time shows again a linear dependence as a function of the reduced volume.

Acknowledgments

This project was supported by The Defense Threat Reduction Agency (DTRA) and The US Army's Edgewood Chemical and Biological Center. The suggestions on the development of the technical framework from Dr. J. Savage, Mr. J. Kiple, and Dr. T. D'Onofrio are greatly appreciated.

References

[1] N.C. Reis Jr., R.F. Griffiths, J.M. Santos, J. Comput. Phys. 198 (2004) 747.
[2] V.M. Starov, Adv. Colloid Interface Sci. 111 (2004) 3.
[3] K.P. Hapgood, J.D. Litster, S.R. Biggs, T. Howes, J. Colloid Interface Sci. 253 (2002) 353.
[4] L.L. Popovich, D.L. Feke, I. Manas-Zloczower, Powder Technol. 104 (1999) 68.
[5] R.K. Holman, M.J. Cima, S.A. Uhland, E. Sachs, J. Colloid Interface Sci. 249 (2002) 432.
[6] V.M. Starov, S.R. Kostvintsev, V.D. Sobolev, M.G. Velarde, S.A. Zhdanov, J. Colloid Interface Sci. 252 (2002) 397.
[7] M. Denesuk, G.L. Smith, B.J.J. Zelinski, N.J. Kreidl, D.R. Uhlmann, J. Colloid Interface Sci. 158 (1993) 114.
[8] N. Alleborn, H. Raszillier, Chem. Eng. Sci. 59 (2004) 2071.
[9] N. Alleborn, H. Raszillier, J. Colloid Interface Sci. 280 (2004) 449.
[10] S.H. Davis, L.M. Hocking, Phys. Fluids 11 (1999) 48.
[11] S.H. Davis, L.M. Hocking, Phys. Fluids 12 (2000) 1646.
[12] H.K. Navaz, B. Markicevic, A.R. Zand, Y. Sikorski, E. Chan, M. Sanders, T.G. D'Onofrio, J. Colloid Interface Sci. 325 (2008) 440.
[13] B. Markicevic, H.K. Navaz, Int. J. Numer. Methods Heat Fluid Flow 19 (2009) 521.
[14] J. Bear, Dynamics of Fluids in Porous Media, Dover Publications, Inc., New York, 1988.